

Multiscale modeling and simulation of traveling waves in biology: a review

W. Duncan Martinson*, Helen M. Byrne and Philip K. Maini

Abstract. *Traveling waves are a near-ubiquitous phenomenon in mathematical biology, and have been studied in the context of embryonic development, cancer growth, wound healing, and epidemiology. Fisher's equation is the prototypical example of a problem that admits a traveling wave solution; it is a partial differential equation that was proposed to describe the spread of an advantageous gene. Although past investigators formulated and analyzed models for such translationally invariant systems at a macroscopic scale of interest, recent work has focused on analyzing and simulating traveling wave behavior in greater detail. This paper reviews the different scales and approaches by which researchers can model and simulate wave-like behavior, using the Fisher equation as a pedagogic example. We discuss different algorithms for simulating traveling waves, from traditional finite difference approaches to more recent hybrid multiscale algorithms.*

1. Introduction

One important class of problems in mathematical biology consists of the identification, modeling, and simulation of systems that exhibit wave-like behavior, i.e. which produce solutions that are invariant with respect to a translation. This type of behavior has been observed in such diverse biological areas as embryonic development [18], neurology [42], population dynamics [74], wound healing [17] and epidemiology [16]. For example, fertilization of an egg cell by a sperm is known to trigger a calcium ion wave throughout the zygote [53]; electrical signals that trigger contractions of the heart can also be modeled as a wave-like phenomenon [43]. Mathematical insight into the generation and propagation of traveling waves may therefore help investigators better understand these natural systems.

The archetypal mathematical model that admits a constant profile, constant speed traveling wave solution is the Fisher Equation, also known as the Fisher-Kolmogorov-Petrovsky-Piskunov (Fisher-KPP) Equation [25]. It is a partial differential equation (PDE) that was originally proposed to model the spread of a gene within a population, although it may also be used to study how any physical, chemical, or biological species spreads over time in a domain with finite resources.

2010 Mathematics Subject Classification: 93C30, 92C42, 65M99, 35C07.

Keywords: Traveling waves, multiscale modeling, hybrid algorithms, Fisher equation.

© The Author(s) 2019. This article is an open access publication.

*Corresponding author.

If $u(x, t)$ measures the density or concentration of such a species at location x and time t , then Fisher's Equation in one dimensional Cartesian coordinates is

$$\frac{\partial u}{\partial t} = D \frac{\partial^2 u}{\partial x^2} + ru \left(1 - \frac{u}{K}\right). \quad (1.1)$$

In Equation (1.1) D , r , and K respectively represent the species' diffusion coefficient, growth rate, and carrying capacity; this last quantity measures the maximum density that the domain can support. Fisher's Equation admits spatially uniform steady state solutions $u = 0$ and $u = K$ (subject to boundary conditions). It has been extensively studied by mathematicians as the prototypical model for a wave-like system due to both its simplicity and amenity to analysis. It is thus a powerful paradigm for studying biological systems that admit traveling wave behavior.

Assuming the initial condition $u(x, 0)$ is continuous and has compact support such that

$$u(x, 0) = u_0(x) \geq 0, \quad u_0(x) = \begin{cases} K, & \text{if } x \leq x_1 \\ 0, & \text{if } x \geq x_2 \end{cases}$$

for some $x_1 < x_2$, with boundary conditions

$$\lim_{x \rightarrow -\infty} u(x, t) = K \quad \text{and} \quad \lim_{x \rightarrow \infty} u(x, t) = 0,$$

then it can be shown that the solution will evolve to a traveling wavefront solution with minimum constant speed c [53]. One can make the change of variables $z = x - ct$ in Equation (1.1) to search for solutions of the form $u(x, t) = U(z)$. This reduces Fisher's Equation to the second-order ordinary differential equation

$$DU'' + cU' + rU \left(1 - \frac{U}{K}\right) = 0, \quad \lim_{z \rightarrow \infty} U(z) = 0, \quad \lim_{z \rightarrow -\infty} U(z) = K. \quad (1.2)$$

The solutions for U and $\frac{dU}{dz}$ may be visualized in the phase plane, and a linear stability analysis about the equilibria $(U, \frac{dU}{dz}) = \{(0, 0), (K, 0)\}$ shows that non-negative traveling wave solutions are possible if $c \geq 2\sqrt{rD}$. For a further discussion of analytical results for Fisher's Equation, we refer to [24] and [53].

The analysis used to estimate the wave speed for Equation (1.1) is performed at the leading edge of the wave front, where $0 < u(x, t) \ll K$; the dynamics behind the wave front (where $u(x, t) = K$) do not contribute to the estimate of the wave speed. In this case, one describes the wave as having a "pulled" front [58]. In contrast, "pushed" fronts occur when dynamics behind the wave front contribute to its velocity. Pushed fronts can occur in any system that has wave-like behavior, and are not only found in the one described by Equation (1.1).

Investigating traveling wave solutions with pulled fronts presents a challenge for researchers for two reasons. Firstly, certain parameter regimes may make the wave front very steep and thus numerically difficult to simulate. In the case of Equation (1.1) for example, it has been found that the gradient of the wave front is inversely

proportional to its speed c [53]. Secondly, in many biological applications the local dynamics near the wave front may not necessarily be appropriately modeled by a PDE. Continuous models describe the change in a macroscopic-level quantity that can be readily observed, for example the density of cells. They can be derived from discrete agent-based models (ABMs) that describe the quantity's corresponding microscopic-level representation (e.g., individual cells) by utilizing a mean-field approximation. This assumes that on average, within a given region of space, there is a sufficiently large number of agents such that they can be represented by a continuous distribution [56]; examples of discrete-to-continuum model derivations are given in [55, 21]. Although this assumption is generally valid in areas such as chemical kinetics, where billions of molecules are present, in many biological applications the number of individuals may be too low to justify a continuum approximation. In such cases, it may be more appropriate to use ABMs to capture a wave front that is commensurate with the scale of the problem.

ABMs can provide finer-scale results than PDE models, incorporate stochastic effects (which can be particularly significant at low densities), be developed from experimental observation, and do not require the use of a mean-field approximation [8, 35, 3, 61]. However, ABMs can be costly to simulate: the time it takes for an algorithm to compute a realization of the model generally increases with the number of agents [33, 62]. Furthermore, investigators have found that ABM simulations for the system modeled by Equation (1.1) exhibit wave speeds slower than that of the mean-field continuum model [62]. Although the average solution to the ABMs for Fisher's Equation can be shown to converge to Equation (1.1) as the number of agents and realizations increase, the rate of this convergence can be slow [62].

These facts have motivated researchers to develop so-called spatially extended hybrid algorithms, which aim to reduce the computational cost of ABM simulation by utilizing equivalent models that differ from each other based on their level of description [68]. By using fine-level models close to the wave front and coarser descriptions in the back, where the mean-field model is likely to be valid, it is possible to accelerate computational speed whilst retaining the fine characteristics of the wave front.

In this paper we review multiscale approaches to simulate systems with wave-like behavior, focusing on the paradigm example of Fisher's Equation. After comparing several basic methods for simulating Equation (1.1) and its equivalent ABMs, we present the different modeling scales and classes of multiscale hybrid algorithms. Finally, we discuss a potential application of these algorithms in the context of cancer biology. We note that this review is not a comprehensive survey of every algorithm that can simulate traveling waves; instead it aims to provide an overview of the different approaches mathematicians can use to investigate translationally invariant systems with inherent multiscale behavior.

2. Basic Numerical Methods for Traveling Wave Simulation

A variety of numerical methods have been proposed to generate traveling wave solutions to PDEs. Table 1 presents representative schematics of basic algorithms that can simulate (or assist in simulating) Equation (1.1). The figures include a plot of the analytic solution to Equation (1.1) at some time $t_n > 0$, subject to the initial and boundary conditions

$$u(x, 0) = Ke^{-x} \quad \forall x \in [0, \infty), \quad u(0, t) = K, \quad \lim_{x \rightarrow \infty} u(x, t) = 0.$$

For this set of initial and boundary conditions, the wave front profile asymptotically approaches $u(x, t) = K(1 + e^{x-ct}/c)^{-1}$ to leading order [53]. This representative profile is sketched as a dotted line, while open circles represent the solution found by each algorithm. Advantages and disadvantages of each numerical method are outlined in Table 2. In this review, we only consider finite difference methods and patch dynamics to solve Equation (1.1), however in practice the Finite Volume Method (FVM) [23], Finite Element Method (FEM) [19], or Method of Lines (MOL) [65] may also be used. The middle row of Table 1 presents a numerical method that has been developed to support the FDM/FVM/FEM in computing solutions to Equation (1.1); it adaptively decomposes the spatial domain to reduce computational complexity.

2.1. Finite Difference Methods

Perhaps the simplest technique for solving PDEs is the finite difference method (FDM), which discretizes a space-time domain into a finite set of regularly-spaced points in order to approximate the continuous PDE (such a set is called a uniform mesh) [69]. Derivatives are estimated using difference schemes located at mesh points. The simplest uniform mesh FDM is the forward Euler scheme, which uses a forward difference for first derivatives and a central difference for second derivatives [69]. We divide the finite spatial domain $[0, L]$ into $M + 1$ points x_i where $0 = x_0 < x_1 = \Delta x < \dots < x_M = M\Delta x = L$. If u_i^n denotes the numerical solution to Equation (1.1) at mesh point x_i and time t_n , $t_n = n\Delta t$, then $\forall n$ the forward Euler method for Equation (1.1) is given by

$$u_i^{n+1} = u_i^n + \frac{D\Delta t}{\Delta x^2}(u_{i+1}^n - 2u_i^n + u_{i-1}^n) + \Delta t \cdot ru_i^n \left(1 - \frac{u_i^n}{K}\right), \quad 0 < i < M. \quad (2.1)$$

The initial condition u_i^0 is found by evaluating the given function $u(x, 0)$ at each mesh point x_i . Equation (2.1) is only valid at internal mesh points; at the boundaries, we must determine discrete analogues of whatever boundary conditions are used to close Equation (1.1). For example, continuous Dirichlet conditions

$$u(0, t) = u_0(t), \quad u(L, t) = u_L(t)$$

are implemented by evaluating $u_0(t)$ and $u_L(t)$ at each t_n . Alternatively, if Neumann boundary conditions are required we can modify Equation (2.1) directly:

Table 1: Spatial Discretization Methods: Representative Plots at $t = t_n$. For each algorithm, the black dotted line represents the approximate wave front to Equation (1.1), while circles represent the numerical solution (initial and boundary conditions are given in the text). Details of each scheme are presented in Section 2. The online article contains a colored version of Table 1.

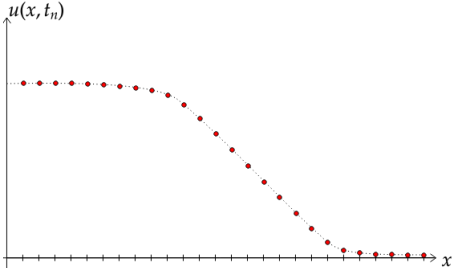
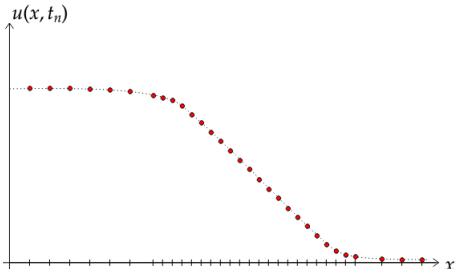
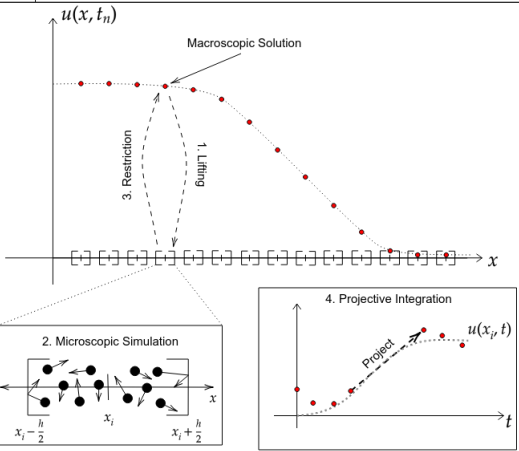
Algorithm	Schematic
Finite Difference Method, with Uniform Mesh	
Finite Difference Method, with Adaptive Mesh	
Patch Dynamics	

Table 2: Basic Methods: Advantages and Disadvantages

Algorithm	Advantages	Disadvantages
Finite Difference Method, Uniform Mesh [69]	<ul style="list-style-type: none"> • Simple to Implement • Stability conditions well-known • Schemes of known high-order accuracy are available 	<ul style="list-style-type: none"> • Solution determined only at mesh points • Information is lost if mesh is too coarse • Many mesh points needed for high spatial resolution • A convergent algorithm may be computationally costly
Finite Difference Method, Adaptive Mesh [7, 11]	<ul style="list-style-type: none"> • Local mesh refinement allows focus on regions where solution varies rapidly • Can reduce computational time by decreasing the number of mesh points 	<ul style="list-style-type: none"> • Method of updating mesh point location can be computationally costly • For moving meshes, mesh points may cross • Instability may result if mesh points are too close
Patch Dynamics [63, 64, 39, 45, 47]	<ul style="list-style-type: none"> • Can accelerate ABM simulations to yield macroscopic quantities of interest • Implementation only requires an ABM and methods for converting a microscopic quantity to a macroscopic one and vice versa • Integration can occur in a frame of reference that co-evolves with the traveling wave 	<ul style="list-style-type: none"> • Only more efficient if macroscopic evolution equation is unknown • Time derivative of macroscopic quantity must not change markedly • Can be unclear how to define appropriate boundary conditions • Requires development of problem-specific lifting and restriction operators

a central difference approximation at each boundary shows that if we implement Equation (2.1) at $i = 0$ and $i = M$ with the respective substitutions

$$u_{-1}^n = u_2^n, \quad u_{M-1}^n = u_{M+1}^n,$$

then the flux $\partial u / \partial x$ across the boundaries will become equal to 0.

FDMs reduce the continuous problem to a discrete algebraic system that must be solved at every specified time point. FDMs are simple to implement and also have well-known stability properties. For example, Equation (2.1) is stable at internal mesh points provided [69]

$$\frac{D\Delta t}{\Delta x^2} \leq \frac{1}{2}.$$

Other finite difference schemes such as the Crank-Nicolson method [15] or the backward Euler method [69] have been proven to be unconditionally stable at internal mesh points if uniform spacing is used.

A further property used to compare FDMs is their order of accuracy, which is determined by the schemes' local truncation error. The truncation error, τ , is the error generated by the difference scheme at each time step. As such, it depends on both Δt and Δx [69]. For example, the truncation error τ of Equation (2.1) at internal mesh points is given by

$$\tau = \frac{1}{2}\Delta t \frac{\partial^2 u}{\partial t^2} - \frac{1}{12}\Delta x^2 \frac{\partial^4 u}{\partial x^4} + O(\Delta t^2) + O(\Delta x^4), \quad (2.2)$$

which may be rewritten using O -notation as $O(\Delta t) + O(\Delta x^2)$. FDMs with higher orders of accuracy than Equation (2.1) converge more quickly to the analytic solution than the forward Euler scheme when the time step and/or mesh spacing are decreased. The Crank-Nicolson method is an example of one such higher order scheme; it has a local truncation error of order $O(\Delta t^2) + O(\Delta x^2)$ [15].

Despite these advantages, there are some issues in simulating traveling waves with FDMs. The numerical solution obtained by a FDM is only known at the specified mesh points; solution values elsewhere must be estimated via interpolation. For Fisher's Equation, the fronts of traveling waves can be steep, depending on the initial conditions and model parameters used [53]. If the spatial distance Δx between mesh points is too large, then the FDM may fail to capture important characteristics of the solution. In such cases, refined mesh spacing near the wave front may be needed to fully resolve the solution. If a uniform mesh is used, however, mesh refinement will increase the number of equations that must be solved at each time step; additionally areas both far ahead of and behind the wave front will be greatly resolved. Since the solution values in these latter regions are slowly varying, an excessive amount of computational time is expended tracking "uninteresting" parts of the solution. For conditionally stable methods, the time step Δt may also have to be reduced to ensure that the numerical solution converges to the analytic solution of Equation (1.1) when the mesh is refined.

2.2. Adaptive Mesh Decomposition Algorithms

The above considerations have motivated the development of adaptive meshes for solving PDEs, which aim to achieve the high resolution required to resolve a wave front while limiting computational effort elsewhere [7, 11]. There are two main classes of adaptive meshes, depending on the manner in which the mesh is updated. In h -refinement methods, mesh points are added or removed from the grid based on estimates of the solution error [7]. Although such adaptive algorithms are well-established in the literature, they can be complex to implement and it can be difficult to control how many mesh points are added to the domain [11].

By contrast, r -refinement methods do not change the number of grid points in the mesh; instead they shift their spatial location. Mesh movement is implemented by mapping a uniformly-spaced mesh to a non-uniform grid in which points are more dense in regions of interest. Regions of interest are identified via a monitor function M . The monitor function is designed to equidistribute mesh points; it can depend on the solution's properties (such as arc length or curvature) and/or estimates of the error. For a more extensive discussion of moving mesh algorithms and their implementation, we refer to the review by Budd *et al.* [11].

r -refinement algorithms have several limitations, perhaps the most notable being that the level of solution resolution depends on the number of mesh points. This issue is less severe than in the case of uniform mesh FDMs, however, as the adaptive algorithms will distribute more mesh points near the wave front. Some moving mesh methods ensure the equidistribution of mesh points by introducing additional PDEs that are derived from necessary conditions on the monitor function, however they may increase the computational cost of the algorithm [11]. Mesh entanglement, in which two or more mesh points "cross," may also occur for some moving mesh algorithms [11]. Finally, great care must be taken if an adaptive mesh is used with a conditionally stable FDM, as instability may result if the time step Δt is not also changed. Interestingly, some FDMs which are unconditionally stable at internal mesh points for uniform meshes (such as the Crank-Nicolson method) are only conditionally stable when moving meshes are used [52].

2.3. Patch Dynamics

There may be situations in which an ABM exists for modeling a translationally invariant phenomenon but a continuum model that describes its macroscale behavior does not exist in closed form (although in principle it does exist). In addition, it may not be tractable to simulate the ABM over large biologically relevant scales of space-time: although we may wish to simulate our ABM for some time interval Δt , it may not be possible to do so over the entire spatial domain for longer than k short time intervals of duration δt , with $k\delta t \ll \Delta t$. In such cases, Patch Dynamics (PD) may be a useful algorithm [63, 64, 39, 45, 47]. PD accelerates and coarse-grains simulations of a microscopic-level ABM in order to estimate its equivalent dynamics on the macroscopic scale. In practice, the ABM is simulated

only on small patches of space-time, and the solution is interpolated from these microscopic-level results. The full PD scheme combines three existing algorithms: (i) a coarse time-stepper [72], (ii) a gap-tooth scheme [45], and (iii) projective integration [46].

The coarse-time stepper computes a macroscopic-level solution from the results of a microscopic-level model (this is assumed to be a discrete ABM, but can, in principle, be continuous) [72]. The coarse time-stepper requires four pieces of information: (1) macroscopic initial data (which is assumed to be given), (2) the microscopic model, (3) a “lifting” operator which fine-grains the macroscopic data to generate consistent microscopic initial conditions for the ABM, and (4) a “restriction” operator that coarse-grains ABM results to generate equivalent data on the desired macro-scale. We use the following illustrative example to describe how the coarse-time stepper works. Suppose we wish to know how average cell densities evolve under the influence of chemotaxis, but only have data at some initial time and an ABM that can simulate the movement of individual cells. Using the lifting operator on the cell density data, we can determine the position, velocity, orientation, and so on of individual cells. The ABM is then simulated using these initial data, and at the end of the realization the final states of each cell are used by the restriction operator to determine the cell density profile at this later time point. In this manner, the time stepper estimates the macroscopic behavior of a microscopic ABM.

PD incorporates the coarse time-stepper along with the gap-tooth scheme [45] in order to reduce the number of agents that must be simulated by the ABM. In the gap-tooth scheme, the spatial domain is subdivided into a set of non-overlapping patches, each of size h , whose midpoints lie a distance Δx apart (this requires that $h \leq \Delta x$). In principle the entire domain can be covered by patches, but typically only a fraction of the domain is used in order to accelerate computations. The ABM is simulated only within the patches, and the final results are used by the restriction operator to estimate the macroscopic solution at each patch midpoint (see the schematic in Figure 1) [45, 64]. Since only a fraction of the domain is simulated, interpolation between patches is needed to obtain a globally accurate solution. In practice, this is accomplished by imposing suitable boundary conditions on each patch, and these are constructed as follows for the case of one spatial dimension. If u_i^n represents the macroscopic data at patch i and time t_n , then the spatial gradient of the macroscopic solution midway between two patches is approximated by the following central difference formula:

$$s_{i+1/2} := \left. \frac{\partial u}{\partial x} \right|_{x=(x_i+x_{i+1})/2} \approx \frac{u_{i+1}^n - u_i^n}{\Delta x}. \quad (2.3)$$

The resulting values $s_{i+1/2}$ are then linearly interpolated to approximate the gradient at each patch boundary. The ABM implements these boundary conditions to match the prescribed flux between patches (for examples of implementing reactive boundary conditions for microscopic models, we refer to [32, 22]).

The final algorithm that PD implements is known as projective integration [46],

which uses the properties of stiff differential equations to accurately accelerate numerical solutions by “skipping” forward in time. Stiff differential equations have at least one dependent variable that lies along a “slow manifold,” meaning that its time derivative does not change markedly over long time periods (for instance, over a time period Δt). Other dependent variables will lie along a fast manifold, meaning that their values change rapidly over the short time scale $\delta t \ll \Delta t$. Projective integration accelerates numerical computations of stiff equations by exploiting the slow manifold: after simulating the stiff differential equations for k short time steps of size δt , the time derivative of the slow variable is estimated and the solution extrapolated over the time interval $\Delta t - k\delta t$. One projective algorithm is the forward Euler projection scheme: assuming $u(x_i, t)$ is the macroscopic solution at location x_i and time t , it is given by

$$u(x_i, t + \Delta t) = u(x_i, t + k\delta t) + (\Delta t - k\delta t) \frac{\partial u}{\partial t}, \quad (2.4)$$

$$\frac{\partial u}{\partial t} \approx \frac{u(x_i, t + k\delta t) - u(x_i, t + (k-1)\delta t)}{\delta t}. \quad (2.5)$$

The purpose of running the algorithm for k short time steps is to dampen errors generated after extrapolation: because solutions will converge to the slow manifold, running the algorithm for larger values of k improves the estimate in Equation (2.5). In addition, any errors that result from extrapolation will be small due to the slow manifold, provided the projective algorithm is numerically stable [46].

Although the projective integration algorithm was originally formulated to study stiff differential equations, a framework has been developed to simulate systems with self-similarity and/or constant speed, constant profile traveling wave solutions [41]. Here the projective step is conducted in a co-evolving frame of reference. In the case of Equation (1.1), for example, the macroscopic solution at location x_i and time t_n would first be shifted by $x_i - ct_n$ before projection, where c is the traveling wave speed determined by the parameters of Equation (1.1) (see Section 1). Since traveling wave solutions to Equation (1.1) are invariant in the frame $x - ct$, this ensures that the time derivative of the macroscopic solution does not change much between successive steps of the algorithm.

For each time step of size Δt , the full PD algorithm in one spatial dimension works as follows (see the schematic in Table 1 for a visual representation, and note that the steps listed below correspond to those indicated on the figure):

0. **Calculate Patch Boundary Conditions.** Using local macroscopic data, the spatial gradient at each patch boundary is calculated using Equation (2.3) and linear interpolation.
1. **Lifting/Fine-Graining.** Using the macroscopic-level data, a consistent initial condition is created for the microscopic model.
2. **Microscopic Simulation.** The boundary conditions identified in step (0) are applied at patch endpoints. Using an appropriate stochastic simulation

algorithm [21, 33, 50], the solution is evolved over k time steps of duration δt (see step (4)).

3. **Restriction/Coarse-Graining.** Using the microscopic results, macroscopic solutions are estimated at the k^{th} and $(k - 1)^{\text{th}}$ time points.
4. **Projective Integration.** The time derivative of the macroscopic variable is approximated using Equation (2.5) and used to extrapolate the solution at time $\Delta t \gg (k + 1)\delta t$.

One advantage of using PD is that it can dramatically accelerate ABM simulations; indeed, in [20] the PD algorithm was 1250-2500 times faster at computing solutions for a simple chemotaxis model than traditional stochastic simulation algorithms (SSAs). In addition, the PD solution was qualitatively similar to that found by the ABM. PD represents an efficient and accurate way of simulating the macroscopic behavior of ABMs over long times and spatial distances. However, if one has a closed-form macroscopic model that describes the average large-scale behavior of the ABM, then traditional methods like FDMs are typically much faster at computing solutions. In addition, stability conditions of FDMs are better characterized than those of PD and it is usually clear how to adjust meshes for FDMs to improve solution accuracy.

The multi-layered nature of PD makes controlling errors a difficult process as the mesh spacing, SSA, patch boundary conditions, projective integration scheme, lifting method, and restriction procedure all contribute to the overall error. Attention must be paid to the stability of the gap-tooth scheme and projective integration in order to ensure solution convergence; this may have to be evaluated on a problem-specific basis [45, 46, 20, 41]. In [45], the truncation error of an idealized PD algorithm was found to be of order $O(\Delta t) + O(\Delta x^2) + O(|\Delta x^2 - h^2|)$, where Δt is the macroscopic time interval, Δx is the distance between patch midpoints, and h is the size of a patch. The lifting and restriction operators also tend to be developed on a problem-specific basis, and it may not be evident what functions are appropriate; this can make it difficult to implement the algorithm. Finally, the microscopic states generated by the lifting operator are not necessarily unique, and, therefore, multiple realizations may be needed at each time step in order to capture the system's average behavior.

In an attempt to reduce errors resulting from the imposition of inconsistent patch boundary conditions (step (0) of PD), some authors have introduced “buffer” regions, which lie between the patch boundaries and a “core” region surrounding the patch midpoint [64, 47, 48, 49, 51, 20]. The PD algorithm with buffers is identical to the one outlined above except for two main changes. The first lies within step (0): boundary conditions may be arbitrarily defined on each patch, rather than calculated from local macroscopic data; for example no-flux boundary conditions could be imposed. The other change corresponds to step (3) of the algorithm: only agents that lie within the core region of a given patch are used to develop macroscopic data at its midpoint x_i . The buffer region's size can be taken

as the distance an agent is expected to travel from a patch boundary towards its respective core within the time period $k\delta t$. Numerical artefacts associated with inconsistent boundary conditions are thus less likely to influence the macroscopic solution. A more detailed description of buffer regions is given in Samaey *et al.* [64]. Their article includes a proof of the PD algorithm's convergence to a model diffusion problem in which buffers are used.

3. Multiscale Modeling of Fisher's Equation

In broad terms, mathematical models can be formulated at macroscopic, mesoscopic, and microscopic scales (or combinations thereof). Macroscopic models typically describe systems where a mean-field approximation is assumed to be valid, and thus they describe continuous quantities such as average concentrations or population densities. Models at this scale can therefore be formulated as PDEs or stochastic partial differential equations (SPDEs). Macroscopic models are extremely useful because they usually measure experimentally observable quantities, have a large body of research dedicated to their simulation (see Section 2 for examples), and tend to be analytically tractable. For example, the minimum wave speed of Equation (1.1) can be defined in terms of the model parameters r and D . Macroscopic models do however have their disadvantages: as previously mentioned, the mean-field approximation may cease to be valid at low concentrations, and thus the (S)PDE may not be accurate in regions with small solution values. This can result in the model overestimating or even underestimating traveling wave speeds [62]. In addition, macroscopic models cannot provide the locations of specific agents, as they only describe the average behavior of a system. If a deterministic PDE is used as a macroscopic model, then stochastic effects that occur in nature are not taken into account (although they can be included in SPDEs). Macroscopic models thus sacrifice potentially important biological detail for computational and analytical tractability.

Microscopic models can be thought of as the opposite of macroscopic models: they provide very detailed descriptions of biological behavior at the cost of analytic and computational tractability. Microscopic models track the locations of individual agents: for "on-lattice" models, individuals occupy prescribed grid sites, while for "off-lattice" models, position is represented as a continuous variable (both types of models can be formulated in one or more spatial dimensions). These systems are simulated using stochastic simulation algorithms (SSAs) such as the Gillespie algorithm [34, 21, 33] or a discretized stochastic differential equation (SDE) [50]. Models at this scale are usually straightforward to construct and implement, and can readily account for effects like volume exclusion [60]. However, simulation times increase with the number of agents. Due to the presence of noise, these models tend to be harder to analyze than PDEs: it may not be possible to derive a continuous, closed-form macroscopic model. In situations where a continuum description of the microscopic model can be derived (as for Equation (1.1)),

multiple realizations of the microscopic model may be needed to converge to the macroscopic solution, and the rate of this convergence can be slow [62].

Mesoscopic models can be regarded as a “halfway point” between macroscopic and microscopic systems: they provide more detailed information than macroscopic models but are faster to simulate than microscopic ones. To model Equation (1.1) in this manner, we will consider a homogeneous population of identical agents that are moving in one spatial dimension and subject to birth and death processes (extension to multiple spatial dimensions is straightforward). Such mesoscopic systems are often termed compartment-based models because they track agent numbers within specific regions; the dependent variable is thus discrete rather than continuous. The Gillespie SSA or a version of it [34, 21, 33] is used to simulate these systems. Each compartment is treated as a chemical species in a reaction network. For example, particles move between adjacent compartments at a rate proportional to their diffusion coefficient. Within each compartment, they are created at rate r , which is the same value as the one in Equation (1.1); similarly, particles are destroyed at a rate such that the average carrying capacity behind the wave front is equal to K from Equation (1.1). The average number of particles in each compartment will evolve according to a chemical master equation, which facilitates the analysis of these models. As the number of agents and realizations of the SSA increase, the master equation converges to a mean-field macroscopic model. Therefore, continuous systems can be derived from mesoscopic models and vice versa. In certain cases however, stochastic effects may preclude derivation of closed-form results. Another limitation of mesoscopic models is that they cannot determine the precise location of an agent in space, although they can identify a small spatial region in which the agent can be found. These models are therefore less detailed than microscopic ones. In addition, the time for a SSA to compute a realization of the system increases with the number of agents, thus mesoscopic models are slower to simulate than macroscopic ones. For mesoscopic models of Equation (1.1), it is known that the wave speed depends on the number of agents in compartments near the wave front [62, 10, 73]. It may also be the case that mesoscopic models will overestimate traveling wave speeds of other biological systems. As for microscopic models, the mesoscopic solution may converge slowly to its chemical master equation, and many realizations of the SSA may be required.

Table 3 contains representative schematics of all three modeling scales discussed above. Table 4 contains summaries of each scale’s respective advantages and disadvantages, which are further elaborated in the above discussion.

4. Hybrid Multiscale Modeling and Simulation

Given the difficulties of simulating mesoscopic and microscopic models with large numbers of agents and the lack of detailed information in macroscopic ones, recent efforts have focused on developing multiscale hybrid simulation algorithms, which model and simulate a single dependent variable at two different scales of

Table 3: Modeling Scales: Representative Schematics and Assumptions. u represents average population density, while N_{agents} represents number of agents within a compartment. All graphs depict the solution to the 1D Fisher Equation with the same initial and boundary conditions as the figures in Table 1.

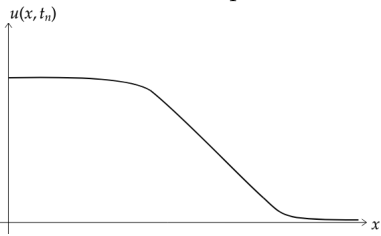
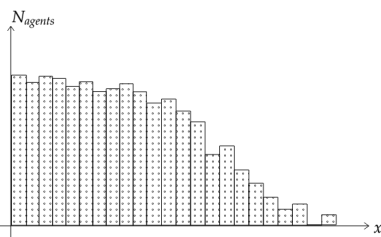
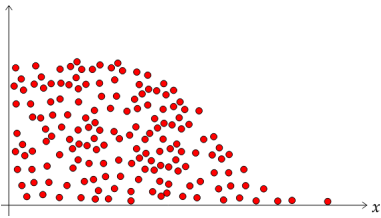
Scale and Representative Schematic	Assumptions, Types of Algorithms Used
<p style="text-align: center;">Macroscopic</p> 	<ul style="list-style-type: none"> • Mean-field Approximation is assumed to be valid • Continuous variable (PDE or SPDE) • Tracks average concentration/density
<p style="text-align: center;">Mesoscopic</p> 	<ul style="list-style-type: none"> • Tracks number of agents within a given spatial region • Discrete variable (SSAs find solutions) • Master equation approaches mean-field model in limit
<p style="text-align: center;">Microscopic</p> 	<ul style="list-style-type: none"> • Discrete variable, tracks positions of all agents • Each agent updated using discretized stochastic differential equation

Table 4: Modeling Scales: Advantages and Disadvantages

Scale	Advantages	Disadvantages
Macroscopic	<ul style="list-style-type: none"> • Can be deterministic or stochastic • More analytically tractable • Closed-form solutions may exist 	<ul style="list-style-type: none"> • Mean-field approximation not always valid • Effect of noise neglected • Does not give information on individual agents • Wave speed may differ from those of microscopic models
Mesoscopic	<ul style="list-style-type: none"> • Gives more information on agent location than macroscopic models • Incorporates noise • Simulations faster than microscopic models 	<ul style="list-style-type: none"> • Wave speed depends on number of agents per compartment • Not possible to track individual agents • Convergence to mean-field can be slow
Microscopic	<ul style="list-style-type: none"> • Most biological description • Can account for cellular-level events • Models usually straightforward to develop 	<ul style="list-style-type: none"> • Very computationally costly • May not be analytically tractable • Discrete-to-continuum limit may not exist

representation [68]. Such algorithms seek to provide the same fine-grained results as microscopic or mesoscopic models in certain parts of the domain, whilst providing computational tractability by having larger-scale models elsewhere. The algorithms can be divided into three main categories, depending on which scales are used: macroscopic-microscopic, mesoscopic-microscopic, and macroscopic-microscopic hybrid algorithms (see Tables 5 and 6). For a more detailed review of these methods, we refer to the paper by Smith *et al.* [68].

4.1. Macroscopic-Mesoscopic Hybrid Algorithms

Macroscopic-mesoscopic algorithms decompose a spatial domain into two regions: in one, a PDE or SPDE is used to model the system's behavior, while in the other a compartment-based model tracks individuals. In the schematic in Table 5, the macroscopic and mesoscopic regions are denoted by Ω_P and Ω_C , respectively. The algorithm depicted is the Pseudo-compartment Method (PCM) originally described by Yates *et al.* [76]. The domains Ω_P and Ω_C are determined as follows: if the concentration of individuals within a compartment is lower than some predefined threshold value, then the mesoscopic description is used and solved with a SSA, otherwise the macroscopic model is simulated using an established method for solving (S)PDEs (see the previous sections). The threshold value is arbitrarily defined and taken to be a value above which a mean-field approximation is likely to hold. Macroscopic-mesoscopic algorithms provide more information about agent locations than (S)PDEs, although they are not as detailed as microscopic ABMs. They are able to account for stochastic effects at low concentrations near the wave front due to the use of a mesoscopic model in that region. The use of a mean-field model is better justified because the macroscopic model is only simulated in regions of high agent density. These algorithms are also faster to simulate than fully mesoscopic models, since the existence of a PDE region reduces the number of agents that need to be simulated by the compartment-based model.

Macroscopic-mesoscopic models have weaknesses, the most obvious being that the precise locations of individual agents are still indeterminate. The wave speed found in Ω_C may still depend on the number of agents per compartment in the vicinity of the wave front, like for fully mesoscopic models. In addition, convergence of the hybrid algorithm to the mean-field model may be slow and require large numbers of agents and realizations. Since particles are transferred stochastically between Ω_C and Ω_P , for each single realization of the algorithm there will be some errors near the interface between the two regions [68].

Specific macroscopic-mesoscopic algorithms differ in how they couple Ω_P and Ω_C to reduce miscalculations of the flux across their shared interface. In the Pseudo-compartment Method [76], a fictitious compartment exists in the PDE region Ω_P , and particles are transferred between the two regions according to the rules of the mesoscopic model. A different method by Harrison *et al.* [37] imagines a region in which the PDE description and compartment model overlap. More examples of coupling conditions are found in the review by Smith *et al.* [68].

Table 5: Hybrid Multiscale Algorithms: Representative Schematics. All graphs model the 1D Fisher Equation with the same initial and boundary conditions as the figures in Table 1.

Algorithm	Schematic
Macroscopic-Mesoscopic Hybrid Algorithm [37, 68, 76]	
Mesoscopic-Microscopic Hybrid Algorithm [62, 26, 27, 28, 68]	
Macroscopic-Microscopic Hybrid Algorithm [67, 68]	

4.2. Mesoscopic-Microscopic Hybrid Algorithms

In contrast to macroscopic-mesoscopic schemes, mesoscopic-microscopic hybrid algorithms do not use a deterministic description anywhere in the domain. Instead, the solution is divided into two regions Ω_C and Ω_B , in which the mesoscopic and

Table 6: Hybrid Multiscale Algorithms: Advantages and Disadvantages

Algorithm	Advantages	Disadvantages
Macroscopic-Mesoscopic Hybrid Algorithm	<ul style="list-style-type: none"> • More detailed representation than PDE models/algorithms • Faster to simulate than mesoscopic algorithms (SSAs) • Can study effects of biological noise 	<ul style="list-style-type: none"> • Cannot track locations of individual agents • Wave speed near front depends on average number of agents per compartment • Convergence to mean-field model can be slow • Numerical error near interface due to flux estimation
Mesoscopic-Microscopic Hybrid Algorithm	<ul style="list-style-type: none"> • Can track precise locations of agents near wave front • More computationally tractable than microscopic simulation • Algorithms are adaptive and can be run in multiple spatial dimensions 	<ul style="list-style-type: none"> • Simulation time is proportional to the number of agents • For certain methods, convergence occurs if compartment size $h \sim \Delta t$, the time step of the microscopic model • Numerical errors may arise due to flux estimation across interface
Macroscopic-Microscopic Hybrid Algorithm	<ul style="list-style-type: none"> • Same computational advantages as macroscopic-mesoscopic algorithms • The time to simulate behavior behind the wave front is independent of number of agents • Can adaptively track locations of individual agents near wave front 	<ul style="list-style-type: none"> • Not always evident how to best couple PDE to microscopic models • Can be a challenge to find an algorithm that correctly couples continuous and discrete variables

microscopic models for behavior are respectively solved. As in the previous class of algorithms, the microscopic model is used if the number of agents within a compartment length from the shared interface is less than an arbitrary threshold value, otherwise the mesoscopic compartment-based model is simulated. These algorithms thus provide the same fine-level detail near the wave front as a complete microscopic model. In addition, because compartment-based models are faster to simulate than particle-based ones, these algorithms compute a solution faster than a full microscopic model. Some mesoscopic-microscopic algorithms are adaptive [62, 28] and thus are well-suited to simulate traveling waves; in addition, there are schemes that can simulate systems in two or more spatial dimensions [28, 27].

All mesoscopic-microscopic algorithms follow the above description but differ specifically on how Ω_C and Ω_B are coupled. For example, in the (adaptive) two-regime method ((A)TRM) [62, 27, 26], particles leave Ω_C at a rate that is designed to make the flux across the shared interface $I = \partial\Omega_C \cap \partial\Omega_B$ consistent with a purely diffusive flux (additional fluxes such as one generated by chemotaxis are similarly implemented). Particles are transferred from Ω_B in two ways: they are absorbed if an agent enters Ω_C within one time step, or they are absorbed with a probability P that measures how likely a particle beginning in Ω_B enters and then leaves Ω_C within one time step. An alternative coupling scheme is given by the Ghost-Cell Method [28] (shown in the schematic in Table 5), in which a fictitious compartment exists within the microscopic region Ω_B , and particles are transferred across I according to the mesoscopic model's rules.

One of the main disadvantages of using mesoscopic-microscopic algorithms is that the time to compute a solution is proportional to the number of agents [68]. In addition, convergence to a continuous mean-field model (if it exists) can be slow and may require many realizations. It has been shown that for some algorithms, this convergence only occurs if $h \sim \Delta t$ and $\Delta t \rightarrow 0$, where h represents the length of a compartment in the mesoscopic model and Δt is the time step of the microscopic model (this is the case for the (A)TRM, but not the Ghost Cell Method, in which only $\Delta t \rightarrow 0$ is required to ensure convergence) [28].

4.3. Macroscopic-Microscopic Hybrid Algorithms

The last multiscale hybrid algorithms that we consider are macroscopic-microscopic methods. These are nearly identical to macroscopic-mesoscopic algorithms, but instead of having a compartment-based model, a microscopic ABM is used in the region Ω_B . Algorithms are distinguished by how they couple the macroscopic domain (Ω_P) with the microscopic domain (Ω_B). For example, the auxiliary region method (ARM, pictured in the schematic in Table 5) [67] couples the regions in a manner similar to the Ghost-Cell and Pseudo-compartment Methods, in that two fictitious compartments are assumed to exist in Ω_P and Ω_B . The flux between these two compartments is governed by the rules of a mathematically consistent mesoscopic model. An alternate algorithm presented by Franz *et al.* [31] takes particles that have crossed into Ω_P within one time step Δt to be equivalent to

continuous Dirac δ -functions, while the PDE solution is allowed to “spill out” into Ω_B . The PDE solution’s integral within Ω_B is, with the appropriate scaling, taken to be equivalent to the probability of creating a new particle in Ω_B [31].

Macroscopic-microscopic hybrid algorithms provide the same computational advantages as macroscopic-mesoscopic methods, except that individual particles near the wave front may now be tracked. Since mesoscopic models are not used behind the wave front, the time that it takes to simulate this part of a traveling wave will not depend on the number of agents being simulated. Some algorithms of this type are adaptive, and therefore can reduce the number of agents that must be simulated in Ω_B even further [68, 67].

One major concern in using macroscopic-microscopic algorithms is how to correctly couple the continuum and discrete models being used: it is still an open question how to best accomplish this task [68]. For example, the average solution of Franz *et al.*’s algorithm converges to the mean-field macroscopic model, but it has been discovered that an overlap region in which the PDE and particle-based model co-exist is required to match the hybrid algorithm’s variance with that of the microscopic model [31]. The existence of an overlap region creates technical issues as it is not clear how to represent bimolecular reactions, since one agent may be represented by the continuum model and another by the microscopic one.

5. Applications and Discussion

In this article, we have reviewed several methods for modeling and simulating systems that exhibit wave-like behavior. We began with a discussion of established algorithms that can simulate behavior at the macroscopic level, ranging from finite difference methods to patch dynamics (although the PD algorithm directly simulates a microscopic ABM, numerical solutions are represented at the macroscopic level). After comparing the three main scales at which multiscale hybrid algorithms are constructed, we then presented several schemes that can utilize detailed descriptions of biological behavior near the wave front whilst maintaining computational tractability by using coarser models elsewhere. Such an approach maximizes the benefits of modeling systems at a fine scale while simultaneously minimizing the computational costs of doing so. In addition, many hybrid algorithms have adaptive frameworks that facilitate tracking of traveling wave solutions. Therefore, hybrid multiscale algorithms offer the possibility of efficient detailed simulation of systems that exhibit wave-like behavior.

As a practical example of a system in which hybrid multiscale algorithms can be applied, we now consider the phenomenon of angiogenesis, the process by which new blood vessels are created from existing vascular networks [29, 36, 75]. Angiogenesis is important in cancer biology, as tumors can stimulate angiogenesis by releasing tumor angiogenic factors (TAFs) such as vascular endothelial growth factor (VEGF), which activate endothelial tip cells lining the walls of existing capillaries [75, 14]. Tip cells move towards the TAF source, creating trails of new

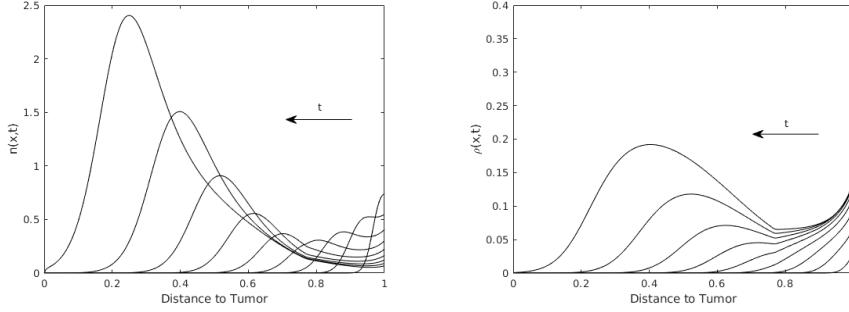


Figure 1: Density of tip cells (left) and vessels (right) given by Equation (5.1) at times $t = \{0.2, 0.4, \dots, 1.8\}$. The tumor is located at $x = 0$, while the parent blood vessel is located at $x = 1$. The parameter values are $\chi = 0.4$, $\alpha_0 = \beta = 50$, $D = 10^{-3}$, $\alpha_1 = 10$, $\nu = 0.2$, $\lambda = 1$, $\gamma = 0.25$. The initial conditions are $n(x, 0) = \rho(x, 0) = 0$ for $0 \leq x < 1$, $n(1, 0) = \rho(1, 0) = 1$, $c(x, 0) = 0$ for $0 < x \leq 1$, $c(0, 0) = 1$. The boundary conditions are $n(1, t) = e^{-1.5t}$, $p(1, t) = 0.05 + 0.95e^{-1.5t}$, $n(0, t) = \rho(0, t) = c(1, t) = 0$, $c(0, t) = 1$.

endothelial cells in their wake [59, 40, 9]. The movement of tip cells (and by extension, endothelial cells) is thought to be dominated by directed chemotaxis rather than random motility [9]. Tip and endothelial cells undergoing angiogenesis have been observed to move in traveling wave-like patterns akin to those of bacterial cells moving chemotactically [1, 44].

Early mathematical models of angiogenesis [5, 12] were phenomenological and formulated at the macroscopic scale. They are generally called “snail-trail” models because the rate of blood vessel formation is assumed to be proportional to the flux of tip cells in the domain. One particular model of angiogenesis that relied on the snail-trail approach was developed by Byrne and Chaplain [12, 13] for a 2D corneal assay. Letting $n(x, t)$ be the density of tip cells at location x and time t , $\rho(x, t)$ the density of blood vessels, and $c(x, t)$ the concentration of TAF, their complete non-dimensionalized system in 1D is given by

$$\begin{aligned} \frac{\partial n}{\partial t} &= D \frac{\partial^2 n}{\partial x^2} - \chi \frac{\partial}{\partial x} \left(n \frac{\partial c}{\partial x} \right) + \alpha_0 \rho c + \alpha_1 n c H(c - \nu) - \beta n \rho, \\ \frac{\partial \rho}{\partial t} &= \left| D \frac{\partial n}{\partial x} - \chi n \frac{\partial c}{\partial x} \right| - \gamma \rho, \\ \frac{\partial c}{\partial t} &= \frac{\partial^2 c}{\partial x^2} - \lambda c - \alpha_1 n c H(c - \nu). \end{aligned} \quad (5.1)$$

Here $H(\cdot)$ is the Heaviside step function, D the diffusion coefficient of cells, χ their chemotactic sensitivity, α_0 their rate of branching from other sprouts, α_1 their branching rate from tip cells, β the rate of tip-elimination by collision with a vessel, γ the rate of vessel pruning and λ the rate of TAF degradation. Results for

both the tip cell and vessel densities are given in Figure 1, from which it is clear that both quantities exhibit traveling wave behavior. Other macroscopic models of angiogenesis did not use the same snail-trail approach as Equation (5.1), but traveling wave solutions to these systems have been identified nevertheless [57]. For a review of other macroscopic models of angiogenesis, we refer to [66].

In contrast to early angiogenesis models, the last twenty years have seen a shift in focus to modeling the cellular-level microscopic behavior of angiogenesis [66, 2]. Two reasons for this shift include the desire to visualize the capillary networks created by such models and to create models inspired by experimental observation. Another important reason is that, as in the Fisher Equation, the dependent variables exhibit low densities in certain regions, calling into question the validity of the continuum (mean-field) model assumption. One of the earliest ABMs for angiogenesis was developed by Anderson and Chaplain [4], via a continuum-to-discrete derivation. Other researchers have developed microscopic models based on stochastic differential equations [71], the cellular Potts model [6], or other considerations [66]. Some have even developed compartment-based models of angiogenesis: Spill *et al.* created a model of this type that was designed to be mathematically consistent with Equation (5.1) [70].

The insights from smaller-scale models of angiogenesis have been limited by the high computational cost of simulating agent-based models. Multiscale approaches are thus increasing in prevalence [2, 66, 38]; in this context, however, “multiscale” refers to the process of modeling different dependent variables at a variety of scales. For example, the concentration of VEGF is typically modeled by a macroscopic PDE, while tip and endothelial cells are simulated via ABMs. This approach differs from the algorithms presented in Section 4, where a single dependent variable was modeled at multiple spatial scales. While the research on single species hybrid algorithms is still in its infancy, the literature on this other type of multiscale simulation is more extensive (for details, see Franz and Erban [30]).

In summary, high-level PDE models for macroscopic behavior have a long history of use in mathematical biology and have advanced our knowledge enormously. In this review, we have raised issues over the validity of these models in the case of their application to intrinsically multiscale processes. We have compared and contrasted a range of modeling and numerical simulation methods that have been developed to address such problems. As we have seen, these pose computational and mathematical challenges when applied to complicated biological processes. An open question that remains to be addressed in the context of traveling wave phenomena is how to evaluate the error induced by the mean-field approximation, and compare it to other modeling errors such as those for parameter estimation.

Acknowledgements. W.D.M. acknowledges funding from the Keasbey Memorial Foundation (postgraduate scholarship)

References

- [1] Adler, J.: Chemotaxis in bacteria. *Science* **153**, 708-716 (1966)
- [2] Alarcón, T.: Modelling tumour-induced angiogenesis: A review of individual-based models and multiscale approaches. *Contemp. Math.* **492**, 45-75 (2009)
- [3] An, G., Mi, Q., Dutta-Moscato, J., Vodovotz, Y.: Agent-based models in translational systems biology. *Wiley Interdiscip. Rev. Syst. Biol. Med.* **1**, 159-171 (2009)
- [4] Anderson, A.R.A., Chaplain, M.A.J.: (1998). Continuous and discrete mathematical models of tumor-induced angiogenesis. *Bull. Math. Biol.* **60**, 857-900 (1998)
- [5] Balding, D., McElwain, D.L.S.: A mathematical model of tumour-induced capillary growth. *J. Theoret. Biol.* **114**, 53-73 (1985)
- [6] Bauer, A.L., Jackson, T.L., Jiang, Y.: A cell-based model exhibiting branching and anastomosis during tumor-induced angiogenesis. *Biophys. J.* **92**, 3105-3121 (2007)
- [7] Berger, M.J., Olinger, J.: Adaptive mesh refinement for hyperbolic partial differential equations. *J. of Comput. Phys.* **53**, 484-512 (1984)
- [8] Black, A.J., McKane, A.J.: Stochastic formulation of ecological models and their applications. *Trends Ecol. Evol.* **27**, 337-345 (2012)
- [9] Bowersox, J.C., Sorgente, N.: Chemotaxis of aortic endothelial cells in response to fibronectin. *Cancer Res.* **42**, 2547-2551 (1982)
- [10] Brunet, E., Derrida, B.: Shift in the velocity of a front due to a cutoff. *Phys. Rev. E* **56**, 2597-2604 (1997)
- [11] Budd, C.J., Huang, W., Russell, R.D.: Adaptivity with moving grids. *Acta Numer.* **18**, 111-241 (2009)
- [12] Byrne, H.M., Chaplain, M.A.J.: Mathematical models for tumour angiogenesis: Numerical simulations and nonlinear wave solutions. *Bull. Math. Biol.* **57**, 461-486 (1995)
- [13] Byrne, H.M., Chaplain, M.A.J.: Explicit solutions of a simplified model of capillary sprout growth during tumour angiogenesis. *Appl. Math. Lett.* **8**, 71-76 (1995)
- [14] Carmeliet, P., Jain, R.K.: Molecular mechanisms and clinical applications of angiogenesis. *Nature* **473**, 298-307 (2011)
- [15] Crank, J., Nicolson, P., Hartree, D.R.: A practical method for numerical evaluation of solutions of partial differential equations of the heat-conduction type. *Math. Proc. Cambridge Philos. Soc.* **43**, 50-67 (1947)
- [16] Cummings, D.A.T., Irizarry, R.A., Huang, N.E., Endy, T.P., Nisalak, A., Ungchusak, K., Burke, D.S.: Travelling waves in the occurrence of dengue haemorrhagic fever in Thailand. *Nature* **427**, 344-347 (2004)
- [17] Dale, P.D., Olsen, L., Maini, P.K., Sherratt, J.A.: Travelling waves in wound healing. *FORMA* **10**, 205-222 (1995)
- [18] Deneke, V.E., Melbinger, A., Vergassola, M., Di Talia, S.: Waves of Cdk1 Activity in S phase synchronize the cell cycle in *Drosophila* Embryos. *Dev. Cell* **38**, 399-412 (2016)
- [19] Elman, H.C., Silvester, D.J., Wathen, A.J.: Finite elements and fast iterative solvers: with applications in incompressible fluid dynamics (2nd ed.). Oxford University Press, New York (2014)
- [20] Erban, R., Kevrekidis, I.G., Othmer, H.G.: An equation-free computational approach for extracting population-level behavior from individual-based models of biological dispersal. *Phys. D* **215**, 1-24 (2006)
- [21] Erban, R., Chapman, J., Maini, P.: A practical guide to stochastic simulations of reaction-diffusion processes. [arXiv:0704.1908](https://arxiv.org/abs/0704.1908) (2007)
- [22] Erban, R., Chapman, S.J.: Reactive boundary conditions for stochastic simulations of reaction-diffusion processes. *Phys. Biol.* **4**, 16-28 (2007)
- [23] Eymard R., Gallouët T., Herbin R.: Finite volume methods. In: *Techniques of Scientific Computing, Part III, Handbook of Numerical Analysis, VII*, pages 713-1020. North-Holland, Amsterdam (2000)
- [24] Fife, P.C., McLeod, J.B.: The approach of solutions of nonlinear diffusion equations to travelling front solutions. *Arch. Ration. Mech. Anal.* **65**, 335-361 (1977)

- [25] Fisher, R.: The wave of advance of advantageous genes. *Ann. Hum. Gen.* **7**, 355-369 (1937); doi:10.1111/j.1469-1809.1937.tb02153.x
- [26] Flegg, M.B., Chapman, S.J., Erban, R.: The two-regime method for optimizing stochastic reaction-diffusion simulations. *J. Roy. Soc. Interface* **9**, 859-868 (2012)
- [27] Flegg, M.B., Chapman, S.J., Zheng, L., Erban, R.: Analysis of the two-regime method on square meshes. *SIAM J. Sci. Comput.* **36**, B561-B588 (2014)
- [28] Flegg, M.B., Hellander, S., Erban, R.: Convergence of methods for coupling of microscopic and mesoscopic reaction-diffusion simulations. *J. Comput. Phys.* **289**, 1-17 (2015)
- [29] Folkman, J.: Angiogenesis in cancer, vascular, rheumatoid and other disease. *Nat. Med.* **1**, 27-30 (1995)
- [30] Franz, B., Erban, R.: Hybrid modelling of individual movement and collective behaviour. In: *Dispersal, individual movement and spatial ecology*, pages 129-157. Springer, Berlin (2013)
- [31] Franz, B., Flegg, M.B., Erban, R., Chapman, S.J.: Multiscale reaction-diffusion algorithms: PDE-assisted Brownian dynamics. *SIAM J. Appl. Math.* **73**, 1224-1247 (2013)
- [32] Gear, C.W., Li, J., Kevrekidis, I.G.: The gap-tooth method in particle simulations. *Phys. Lett. A* **316**, 190-195 (2003)
- [33] Gibson, M.A., Bruck, J.: Efficient exact stochastic simulation of chemical systems with many species and many channels. *J. Phys. Chem. A* **104**, 1876-1889 (2000)
- [34] Gillespie, D.T.: A general method for numerically simulating the stochastic time evolution of coupled chemical reactions. *J. Comput. Phys.* **22**, 403-434 (1976)
- [35] Gillespie, D.T., Hellander, A., Petzold, L.R.: Perspective: Stochastic algorithms for chemical kinetics. *J. Chem. Phys.* **138**, 170901 (2013)
- [36] Gupta, M.K., Qin, R.-Y.: Mechanism and its regulation of tumor-induced angiogenesis. *World J. Gastroenterol.* **9**, 1144-1155 (2003)
- [37] Harrison, J.U., Yates, C.A.: A hybrid algorithm for coupling partial differential equation and compartment-based dynamics. *J. Roy. Soc. Interface* **13**, 20160335 (2016)
- [38] Heck, T.A.M., Vaeyens, M.-M., Van Oosterwyck, H.: Computational models of sprouting angiogenesis and cell migration: towards multiscale mechanochemical models of angiogenesis. *Math. Model. Nat. Phenom.* **10**, 108-141 (2014)
- [39] Hyman, J.M.: Patch dynamics for multiscale problems. *Comput. Sci. Eng.* **7**, 47-53 (2005)
- [40] Jakobsson, L., Franco, C.A., Bentley, K., Collins, R.T., Ponsioen, B., Aspalter, I.M., Gerhardt, H.: Endothelial cells dynamically compete for the tip cell position during angiogenic sprouting. *Nat. Cell Biol.* **12**, 943-953 (2010)
- [41] Kavousanakis, M.E., Erban, R., Boudouvis, A.G., Gear, C.W., Kevrekidis, I.G.: Projective and coarse projective integration for problems with continuous symmetries. *J. Comput. Phys.* **225**, 382-407 (2007)
- [42] Keener, J., Sneyd, J.: *Mathematical physiology I: Cellular physiology* (2nd ed.). Springer, New York (2008)
- [43] Keener, J., Sneyd, J.: *Mathematical physiology II: Systems physiology* (2nd ed.). Springer, New York (2008)
- [44] Keller, E.F., Segel, L.: Traveling bands of chemotactic bacteria: A theoretical analysis. *J. Theoret. Biol.* **30**, 235-248 (1971)
- [45] Kevrekidis, I.G., Gear, C.W., Hyman, J.M., Kevrekidis, P.G., Runborg, O., Theodoropoulos, C.: Equation-free multiscale computation: Enabling microscopic simulators to perform system-level tasks. *Commun. Math. Sci.* **1**, 715-762 (2002)
- [46] Gear, C.W., Kevrekidis, I.G.: Projective methods for stiff differential equations: Problems with gaps in their eigenvalue spectrum. *SIAM J. Sci. Comput.* **24**, 1091-1106 (2003)
- [47] Kevrekidis, I.G., Samaey, G.: Equation-free multiscale computation: algorithms and applications. *Ann. Rev. Phys. Chem.* **60**, 321-344 (2009)
- [48] Lee, S., Kevrekidis, I.G., Karniadakis, G.E.: A resilient and efficient CFD framework: Statistical learning tools for multi-fidelity and heterogeneous information fusion. *J. Comput. Phys.* **344**, 516-533 (2017)
- [49] Lee, S., Kevrekidis, I.G., Karniadakis, G.E.: A general CFD framework for fault-resilient

- simulations based on multi-resolution information fusion. *J. Comput. Phys.* **347**, 290-304 (2017)
- [50] Lipkova, J., Zygalakis, K.C., Chapman, S.J., Erban, R.: Analysis of Brownian dynamics simulations of reversible bimolecular reactions. *SIAM J. Appl. Math.* **71**, 714-730 (2011)
- [51] Liu, P., Samaey, G., Gear, C.W., Kevrekidis, I.G.: On the acceleration of spatially distributed agent-based computations: A patch dynamics scheme. *Appl. Numer. Math.* **92**, 54-69 (2015)
- [52] Mackenzie, J.A., Mekwi, W.R.: An analysis of stability and convergence of a finite-difference discretization of a model parabolic PDE in 1D using a moving mesh. *IMA J. Numer. Anal.* **27**, 507-528 (2007)
- [53] Murray, J.D.: *Mathematical Biology I: An Introduction* (3rd ed.). Springer, New York (2003)
- [54] Murray, J.D.: *Mathematical Biology II: Spatial Models and Biomedical Applications* (3rd ed.). Springer, New York (2003)
- [55] Murray, P.J., Edwards, C.M., Tindall, M.J., Maini, P.K.: From a discrete to a continuum model of cell dynamics in one dimension. *Phys. Rev. E* **80**, 031912 (2009)
- [56] Newman, T.J.: Modeling multi-cellular systems using sub-cellular elements. [arXiv:q-bio/0504028](https://arxiv.org/abs/0504028) (2005)
- [57] Olsen, L., Sherratt, J.A., Maini, P.K., Arnold, F.: A mathematical model for the capillary endothelial cell-extracellular matrix interactions in wound-healing angiogenesis. *Math. Med. Biol.* **14**, 261-281 (1997)
- [58] Panja, D., Beenakker, W. J.: Effects of fluctuations on propagating fronts. *Phys. Rep.* **393**, 87-174 (2004)
- [59] Paweletz, N., Knierim, M.: Tumor-related angiogenesis. *Crit. Rev. Oncol. Hematol.* **9**, 197-242 (1989)
- [60] Pillay, S., Byrne, H.M., Maini, P.K.: The impact of exclusion processes on angiogenesis models. *J. Math. Biol.* **77**, 1721-1759 (2018)
- [61] Rejniak, K.A., Anderson, A.R.A.: Hybrid models of tumor growth. *Wiley Interdisciplinary Reviews: Systems Biology and Medicine* **3**, 115-125, (2011)
- [62] Robinson, M., Flegg, M., Erban, R.: Adaptive two-regime method: Application to front propagation. *J. Chem. Phys.* **140**, 124109 (2014)
- [63] Samaey, G., Roose, D., Kevrekidis, I.G.: Combining the gap-tooth scheme with projective integration: Patch dynamics. In: *Multiscale Methods in Science and Engineering*, pages 225-239. Springer, Berlin (2005)
- [64] Samaey, G., Kevrekidis, I.G., Roose, D.: Patch dynamics with buffers for homogenization problems. *J. Comp. Phys.* **213**, 264-287 (2006)
- [65] Schiesser, W.E.: *The numerical method of lines: Integration of partial differential equations*. Academic Press, San Diego (1991)
- [66] Scianna, M., Bell, C.G., Preziosi, L.: A review of mathematical models for the formation of vascular networks. *J. Theoret. Biol.* **333**, 174-209 (2013)
- [67] Smith, C.A., Yates, C.A.: The auxiliary region method: A hybrid method for coupling PDE-and Brownian-based dynamics for reaction-diffusion systems. *Royal Soc. Open Sci.* **5**, 180920 (2018)
- [68] Smith, C.A., Yates, C.A.: Spatially extended hybrid methods: A review. *J. Roy. Soc. Interface* **15**, 20170931 (2018)
- [69] Smith, G.: *Numerical solution of partial differential equations: finite difference methods*. Oxford University Press, New York (1985)
- [70] Spill, F., Guerrero, P., Alarcon, T., Maini, P.K., Byrne, H.M.: Mesoscopic and continuum modelling of angiogenesis. *J. Math. Biol.* **70**, 485-532 (2015)
- [71] Stokes, C.L., Lauffenburger, D.A., Williams, S.K.: Migration of individual microvessel endothelial cells: stochastic model and parameter measurement. *J. Cell Sci.* **99**, 419-430 (1991)
- [72] Theodoropoulos, C., Qian, Y.-H., Kevrekidis, I.G.: "Coarse" stability and bifurcation analysis using time-steppers: A reaction-diffusion example. *Proc. Nat. Acad. Sci. USA* **97**, 9840-9843 (2000)

- [73] Warren, C., Somfai, E., Sander, L.M.: Velocity of front propagation in 1-dimensional auto-catalytic reactions. *Braz. J. Phys.* **30**, 157-162 (2000)
- [74] Welch, R., Kaiser, D.: Cell behavior in traveling wave patterns of myxobacteria. *Proc. Natl. Acad. Sci. USA* **98**, 14907-14912 (2001)
- [75] Yadav, L., Puri, N., Rastogi, V., Satpute, P., Sharma, V.: Tumour angiogenesis and angiogenic inhibitors: A review. *J. Clin. Diagn. Res.* **9**, XE01-XE05 (2015)
- [76] Yates, C.A., Flegg, M.B.: The pseudo-compartment method for coupling partial differential equation and compartment-based models of diffusion. *J. Roy. Soc. Interf.* **12**, 20150141 (2015)

Received: 22 May 2019/Accepted: 13 July 2019/Published online: 29 August 2019

W. Duncan Martinson

Wolfson Centre for Mathematical Biology, Mathematical Institute, University of Oxford, Woodstock Road, Oxford OX2 6GG, United Kingdom.

william.martinson@maths.ox.ac.uk

Helen M. Byrne

Wolfson Centre for Mathematical Biology, Mathematical Institute, University of Oxford, Woodstock Road, Oxford OX2 6GG, United Kingdom.

helen.byrne@maths.ox.ac.uk

Philip K. Maini

Wolfson Centre for Mathematical Biology, Mathematical Institute, University of Oxford, Woodstock Road, Oxford OX2 6GG, United Kingdom.

philip.maini@maths.ox.ac.uk

Open Access. This article is distributed under the terms of the Creative Commons Attribution 4.0 International License (<http://creativecommons.org/licenses/by/4.0/>), which permits unrestricted use, distribution, and reproduction in any medium, provided you give appropriate credit to the original author(s) and the source, provide a link to the Creative Commons license, and indicate if changes were made.